

. . . , . . . , . . .

, 15, 49005, ; e-mail: ternovayakaterina@gmail.com

(6,5 – 7) %.

()

() , « »

() .

() .

(~ 20)

The goal of this work was to analyze the effect of the corner point of the rocket engine nozzle contour on the nozzle flow characteristics. A two-phase flow in third rocket stage nozzles of different contours was considered. The site of condensed phase deposition onto the wall of a nozzle with an acute angle in the critical area was determined. Rounding the corner point at the supersonic area inlet changed the particle trajectory. The rounding radius best in terms of deposition reduction was found. A comparison showed that, despite the different profiles, the specific impulses of these nozzles differed little from one another and were lower than the specific impulse of the base nozzle by 6.5 - 7%.

The gas flow in nozzles with a corner point at the truncated conical nozzle – bell-shaped tip junction was studied. The flow characteristics were calculated for three nozzle contour configurations in the contour kink area: for an unrounded corner point and for a rounded corner point at the conical nozzle – bell-shaped tip junction. Rounding the corner point at the nozzle – tip junction slightly increases the impulse, although in general it has no significant effect on the wave structure of a particle-free gas flow in a supersonic nozzle.

In terrestrial conditions, the pressure on the wall of the conical supersonic area of a nozzle upstream of the corner point (rounding) sharply decreases to about the same minimum value for different nozzles. In this case, the distance of the pressure minimum from the nozzle throat decreases with increasing rounding radius at the corner point. Thus, the reduced pressure zone on the wall (as compared with the undisturbed pressure in the conical part of the nozzle) extends nearly in proportion to the rounding radius at the corner point. After reaching its minimum value, the pressure gradually increases to its value in the separation zone at approximately the same distance from the nozzle critical section (in the corner point area at the tip inlet).

At high altitudes, the pressure as a function of the corner point rounding radius does not have any pronounced minimum value (with a further increase to the pressure in the separation zone of the tip). For a rounded corner point, the pressure drops as in the previous case (with about the same gradient) and then remains constant and equal to its value in the expansion waves generated when the flow turns in the truncated conical nozzle exit area (about 20 mm downstream of the nozzle throat).

Keywords: truncated nozzle, bell-shaped tip, impulse characteristics, corner point, corner point rounding.

bell n zze» («dual) [1 – 4],

[5, 6].

[7],

[8].

[5, 6].

[5]

m_i ; N ; n_i ; i ;
 ;
 ;
 ;
 ;
 ;

– ;
– ;
– ,

[5]

$$\left. \begin{aligned}
& \nabla \dots \bar{W}y = 0, \\
& \nabla \dots u \bar{W}y + \frac{\partial}{\partial x} yp = y \sum_{i=1}^N \dots_i C_{R_i} (u_i - u), \\
& \nabla \dots v \bar{W}y + \frac{\partial}{\partial y} yp - p = y \sum_{i=1}^N \dots_i C_{R_i} (v_i - v), \\
& \nabla \dots H_0 \bar{W}y = y \sum_{i=1}^N \dots_i \{ C_{a_i} c_p (T_i - T) + C_{R_i} [u_i (u_i - u) + v_i (v_i - v)] \}, \\
& p = \dots RT, H_0 = c_p T + (u^2 + v^2) / 2, \\
& \nabla \dots_i \bar{W}_i y = y [n_i \sum_{j=1}^i \bar{k}_{ij} \dots_{ij} - \dots_i \sum_{j=i}^N \bar{k}_{ij} \dots_{ij} n_j], \\
& \nabla n_i \bar{W}_i y = -y n_i \sum_{i=1}^N \bar{k}_{ij} \dots_{ij} n_j,
\end{aligned} \right\} (1)$$

$$\left. \begin{aligned}
& \nabla \dots_i u_i \bar{W}_i y = y \{ \dots_i C_{R_i} (u - u_i) + n_i \sum_{j=1}^i \bar{k}_{ij} \dots_{ij} [u_j - (1 - \dots_{ij}) u_i] - \dots_i \sum_{j=i}^N \bar{k}_{ij} n_j [u_i - (1 - \dots_{ij}) u_j] \}, \\
& \nabla \dots_i v_i \bar{W}_i y = y \{ \dots_i C_{R_i} (v - v_i) + n_i \sum_{j=1}^i \bar{k}_{ij} \dots_{ij} [v_j - (1 - \dots_{ij}) v_i] - \dots_i \sum_{j=i}^N \bar{k}_{ij} n_j [v_i - (1 - \dots_{ij}) v_j] \}, \\
& \nabla \dots_i E_i \bar{W}_i y = y \{ \dots_i [c_p C_{a_i} (T - T_i) + C_{R_i} [u_i (u_i - u) + v_i (v_i - v)]] + \\
& n_i \sum_{j=1}^i \bar{k}_{ij} \dots_{ij} [E_j - (1 - \dots_{ij}) E_i] - \dots_i \sum_{j=i}^N \bar{k}_{ij} n_j [E_i - (1 - \dots_{ij}) E_j] \}, \\
& E_i = C_{a_i} T_i + (u_i^2 + v_i^2) / 2, \bar{k}_{ij} = k_{ij} \Omega_{ij}, i = 1, \dots, N,
\end{aligned} \right\} (2)$$

$C_{R_i}, C_{a_i} -$; $k_{ij} -$
; $j -$; $\Omega_{ij} -$ -
; $n_i -$ - ; $n_j -$
 $j -$ $i -$; $N -$, $p -$
, $R -$, $i -$;
, $i -$ $i -$; $j -$ $j -$
 $i -$; $p -$, $\bar{W} (u, v) -$ () , - ,
 $u_i v_i -$ $i -$, $E_i -$

$$; E_j - \dots ; u_j, v_j - \dots ; \overline{W} - \dots$$

$$C_{R_i} \dots C_{a_i} \dots [5].$$

$$[9], \dots \Omega_{ij}$$

$$[10], \dots C_{R_i}, k_{ij} [5].$$

$$f(r) = 1 / \sqrt{2f \ln \dagger} \exp[-(\frac{\ln(r/r_0)}{\sqrt{2 \ln \dagger}})^2], \quad (3)$$

$$r - \dots ; r_0, \ln - \dots n_i.$$

$$(1),$$

$$(2), \dots (1)$$

$$\frac{dH_0}{dt} = y \sum_{i=1}^N \dots \{C_{a_i} c_p (T_i - T) + C_{R_i} [u_i (u_i - u) + v_i (v_i - v)]\} \quad (4)$$

$$u > 0 - \dots ; \dots [5]. \quad (2)$$

[5],

(1), (2), (4)

$$(1). \dots (1) \dots (1) \dots (4)$$

$$[5] \dots (4) \dots (2) \dots j- \dots i-$$

$$x_l = x[(1-z) + zC_b / c_p] / [(1=z) + zxC_b / c_p]$$

$Re = (1 - z) \cdot R$, $z =$; $C_b =$
 $;$ - , ; $R =$.

(0,5 - 10)

10

1.

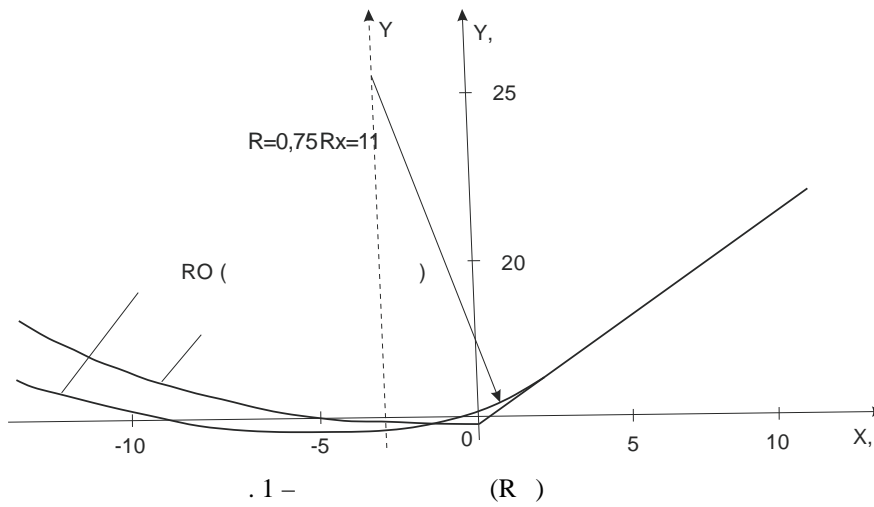
1 -

\bar{x}	0	0,006	0,094	0,05	0,108	0,158	0,218	0,253	0,334
\bar{y}	1	1,003	1,018	1,027	1,06	1,088	1,124	1,145	1,193

0,432	0,552	0,621	0,781	0,874	0,876	1,088	1,5	1,849	2,274
1,254	1,329	1,372	1,474	1,533	1,598	1,67	1,93	2,144	2,397

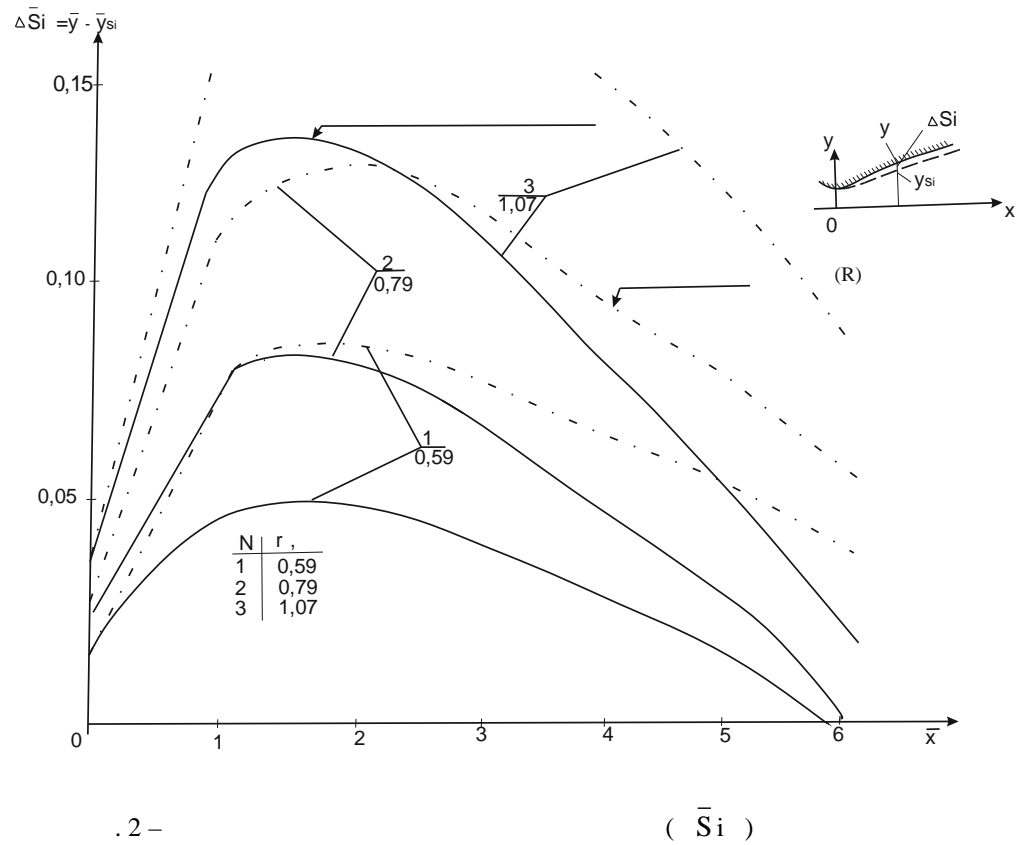
2,791	3,069	3,782	4,182	4,623	5,109	6,237	6,888	7,607	15,19
2,689	2,852	3,2	3,404	3,611	3,829	4,298	4,55	4,811	7,59

1
(R).



$T_o = 3605$, $z = 0,429$, $\mu = 24,74$
 $r_* = 0,145$. $= 7,7$, $= 1,17$

« .2 »
 $\bar{S}_i = \bar{y}(x) - \bar{y}_S$ (x)
 $\bar{y}_S =$
 $r = 0,59$ (1), 0,79
 (2), 1,07 (3)).



. 2 -

(\bar{S}_i)

$\bar{x} \approx 5,7$

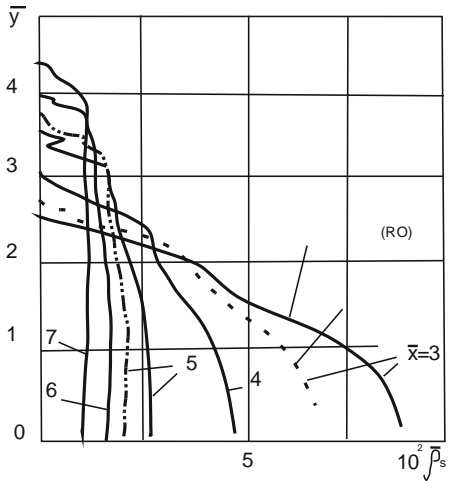
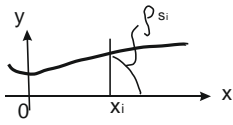
($r = 0,59$)

(. 2)

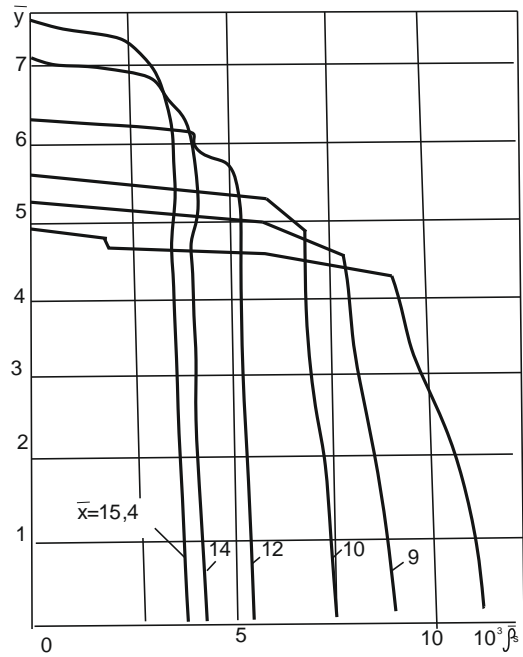
$\bar{R} = 0,75r_*$

S_i

. 3



.3 -



$4L \times 2L,$

$L -$

(. 4).

ANSYS Fluent

(Unsteady Reynolds Averaged Navier-Stokes – URANS)

[12].

$$\sim = \sim_0 \left(\frac{T}{T_0} \right)^{3/2} \frac{T_0 + C}{T + C},$$

$\sim_0 -$

$$\sim_0 = 1,71 \cdot 10^5 \text{ } / \text{ } ^2; C -$$

$$T = T_0 \text{ , } T_0 = 273$$

$$C = 117.$$

—
—
—

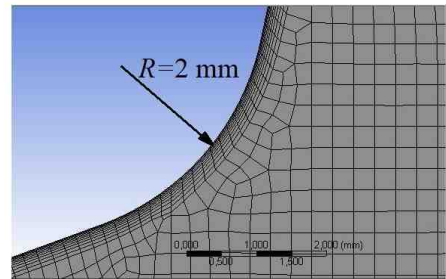
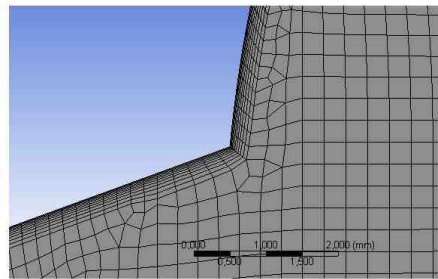
;
,
;

:

$$\frac{R}{r_*} = 0,2 \quad ($$

$R=1$) $0,4$ ($R=2$).

(. 4).



)

)

. 4 -

(- , -)

()

() (~ 10 %)

(. 5,)) .

, « »

()

() .

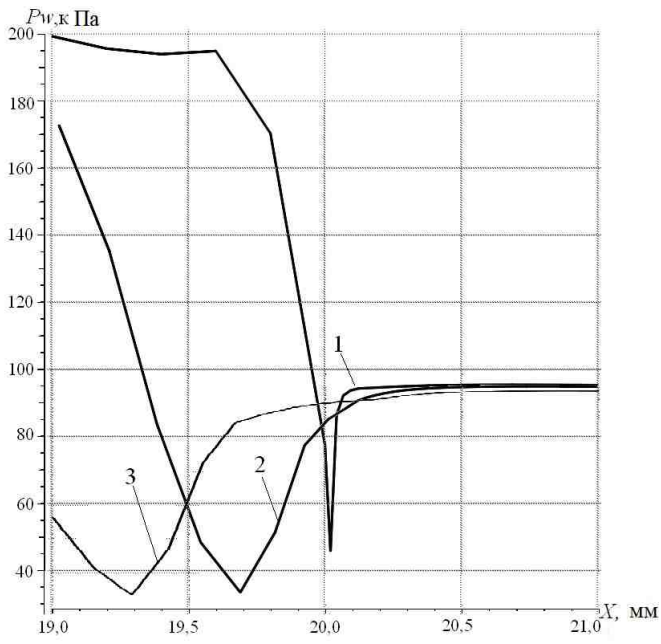
(

) .

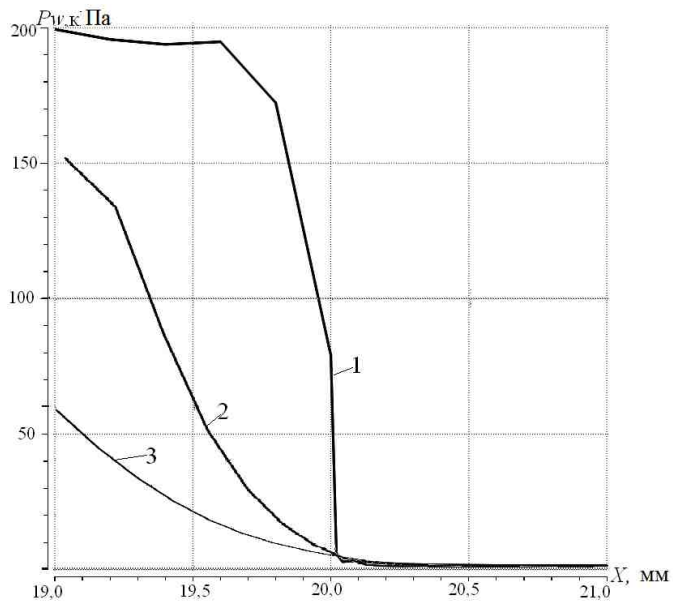
;

(~ 20
(. 5,)) .

)



)



)

.5 - (1), (2) 2 (3)) 10⁴ .

r = 0,59)

$$\bar{R} = 0,75r_*$$

$$\frac{R}{r_*} = 0,2 \quad (R=1) \quad 0,4 \quad (R=2).$$

() () (~ 10 %)

, « » ()

).

(

(),

(~ 20)

1. Arora R., Vaidyanathan A. Experimental investigation of flow through planar double divergent nozzles. *Acta Astronomica*. 2015. 112. P. 200–216. <https://doi.org/10.1016/j.actaastro.2015.03.020>
2. Genin C., Stark R., Haidn O., Quering K., Frey M. Experimental and numerical study of dual bell nozzle flow. *Progr. Flight Phys.* 2013. 5. P. 363–376. <https://doi.org/10.1051/eucass/201305363>
3. Emelyanov V. N., Volkov K. N., Yakovchuk M. S. Unsteady Flow in a Dual-Bell Nozzle with Displacement of an Extendible Section from the Initial to Working Position. *Fluid Dynamics*. 2022. P. 35–45. <https://doi.org/10.1134/S0015462822601267>
4. Hamitouche T., Sellam M., Kbab H., Bergheul S. Design and Wall Fluid Parameters Evaluation of the Dual-Bell Nozzle. *International Journal of Engineering Research and Technology*. 2019. V. 12, 7. P. 1064–1074.
5. . . . , 1993. 223 .
6. . . . , 1993. 191 .
7.
8. Pryadko N. S., Strelnikov G. A., Ternova K. V. Research of supersonic flow in shortened nozzles of rocket engines with a bell-shaped tip. *Space Sci. & Technol.* 2024. 1. . 03–13. <https://doi.org/10.15407/knit2024.01>
9. 1976. 14, 6. . 5–7. <https://doi.org/10.2514/3.61409>
10. , 1974. 212 .
11. , 1966. . 183–201.
12. John E. Matsson. *An Introduction to ANSYS Fluent* 2022. 688 c.

. 23.08.2024,
10.12.2024